Cavitating Inducers

In the presence of cavitation, the transfer function for a pump or inducer will be considerably more complicated than that of equation (Bngi2). Even at low frequencies, the values of TP_{11} will become different from unity, because the head rise will change with the inlet total pressure, as manifest by the nonzero value of $d(\Delta p^T)/dp_1^T$ at a given mass flow rate, m_1. Furthermore, the volume of cavitation, $V_C(p_1^T, m_1)$, will vary with both the inlet total pressure, p_1^T (or $NPSH$ or cavitation number), and with the mass flow rate, m_1 (or with angle of incidence), so that

$$[TP] = \begin{bmatrix} 1 + \frac{d(\Delta p^T)}{dp_1^T}|_{m_1} & \frac{d\Delta p^T}{dm_1}|_{p_1^T} \\ \\ j\omega\rho_L \frac{dV_C}{dp_1^T}|_{m_1} & 1 + j\omega\rho_L \frac{dV_C}{dm_1}|_{p_1^T} \end{bmatrix} \tag{Bngj1}$$

Brennen and Acosta (1973, 1975, 1976) identified this quasistatic or low frequency form for the transfer function of a cavitating pump, and calculated values of the cavitation compliance, $-\rho_L(dV_C/dp_1^T)_{m_1}$ and the cavitation mass flow gain factor, $-\rho_L(dV_C/dm_1)_{p_1^T}$, using the cavitating cascade solution discussed in the section (Mbeu) on "Partially Cavitating Cascades". Both the upper limit of frequency at which this quasistatic approach is valid and the form of the transfer function above this limit cannot readily be determined except by experiment. Though it was clear that experimental measurements of the dynamic transfer functions were required, these early investigations of Brennen and Acosta did highlight the importance of both the compliance and the mass flow gain factor in determining the stability of systems with cavitating pumps.

Ng and Brennen (1978) and Brennen *et al.* (1982) conducted the first experiments to measure the complete transfer function for cavitating inducers. Typical transfer functions are those for the 10.2 *cm* diameter Impeller VI (see the section (Mbbi)), whose noncavitating steady state performance was presented in section (Mben). Transfer matrices for that inducer are presented in figure 1 as a function of frequency (up to 32 *Hz*), for a speed of 6000 *rpm*, a flow coefficient $\phi_1 = 0.07$ and for five different cavitation numbers ranging from data set A that was taken under noncavitating conditions, to data set C that showed a little cavitation, to data set H that was close to breakdown. The real and imaginary parts are represented by the solid and dashed lines, respectively. Note, first, that, in the absence of cavitation (Case A), the transfer function is fairly close to the anticipated form of equation (Bngi2) in which $TP_{11} = TP_{22} = 1$, $TP_{21} = 0$. Also, the impedance (TP_{12}) is comprised of an expected inertance (the imaginary part of TP_{12} is linear in frequency) and a resistance (real part of $-TP_{12}$) which is consistent with the quasistatic resistance from the slope of the head rise characteristic (shown by the arrow in figure 1 at $TP_{12}R_{T1}/\Omega = 1.07$). The resistance appears to increase with increasing frequency, a trend which is consistent with the centrifugal pump measurements of Anderson, Blade and Stevans (1971) which were presented in section (Bngi).

It is also clear from figure 1 that, as the cavitation develops, the transfer function departs significantly from the form of equation (Bngi2). One observes that TP_{11} and TP_{22} depart from unity, and develop nonzero imaginary parts that are fairly linear with frequency. Also TP_{21} becomes nonzero, and, in particular, exhibits a compliance which clearly increases with decreasing cavitation number. All of these changes mean that the determinant, D_{TP}, departs from unity as the cavitation becomes more extensive. This is illustrated in figure 2, which shows the determinant corresponding to the data of figure 1. Note that $D_{TP} \approx 1$ for the non-cavitating case A, but that it progressively deviates from unity as the cavitation increases. We can conclude that the presence of cavitation can cause a pump to assume potentially active dynamic characteristics when it would otherwise be dynamically passive.

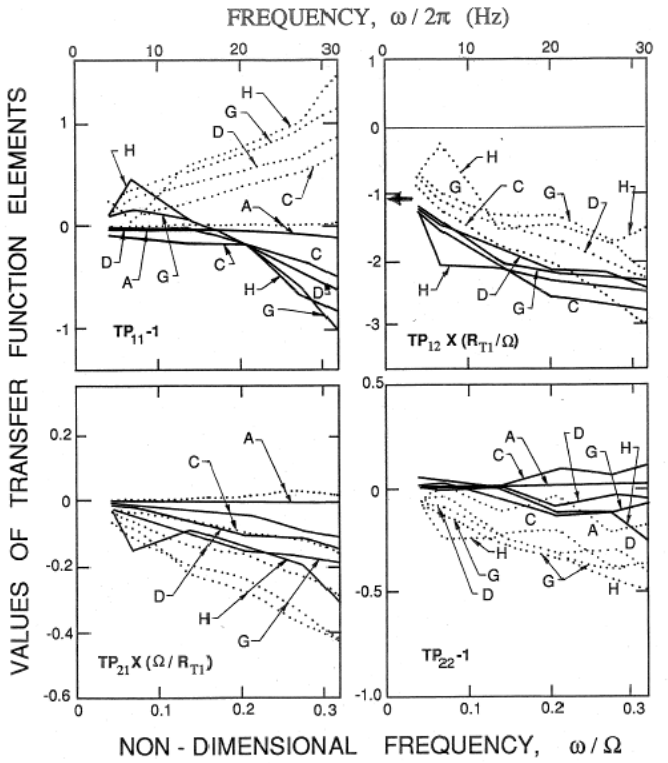

Figure 1: Typical transfer functions for a cavitating inducer obtained by Brennen *et al.* (1982) for a 10.2 *cm* diameter inducer (Impeller VI) operating at 6000 *rpm* and a flow coefficient of $\phi_1 = 0.07$. Data is shown for four different cavitation numbers, σ = (A) 0.37, (C) 0.10, (D) 0.069, (G) 0.052 and (H) 0.044. Real and imaginary parts are denoted by the solid and dashed lines respectively. The quasistatic pump resistance is indicated by the arrow (adapted from Brennen *et al.* 1982).

Polynomials of the form

$$TP_{ij} = \sum_{n=0}^{n^*} A_{nij}(j\omega)^n \tag{Bngj2}$$

were fitted to the experimental transfer function data using values of n^* of 3 or 5. To illustrate the result of such curve fitting we include figure 3, which depicts the result of curve fitting figure 1. We now proceed to examine several of the coefficients A_{nij} that are of particular interest (note that $A_{011} = A_{022} = 1$, $A_{021} = 0$ for reasons described earlier). We begin with the inertance, $-A_{112}$, which is presented nondimensionally in figure 4. Though there is significant scatter at the lower cavitation numbers, the two different sizes of inducer pump appear to yield similar dimensionless inertances. Moreover, the data suggest some decrease in the inertance with decreasing σ. On the other hand, the corresponding data for the compliance, $-A_{121}$, which is presented in figure 5 seems roughly inversely proportional to the cavitation number. And the same is true for both the mass flow gain factor, $-A_{122}$, and the coefficient that defines the slope of the imaginary part of TP_{11}, A_{111}; these are presented in figures 6 and 7, respectively. All of these data appear to conform to the physical scaling implicit in the nondimensionalization of each of the dynamic characteristics.

It is also valuable to consider the results of figures 4 to 7 in the context of an analytical model for the dynamics of cavitating pumps (Brennen 1978). We present here a brief physical description of that model, the essence of which is depicted schematically in figure 8, which shows a developed, cylindrical surface within the inducer. The cavitation is modeled as a bubbly mixture which extends over a fraction, ϵ, of the length, c, of each blade passage before collapsing at a point where the pressure has risen to a value which causes collapse. The mean void fraction of the bubbly mixture is denoted by α_0. Thus far we have

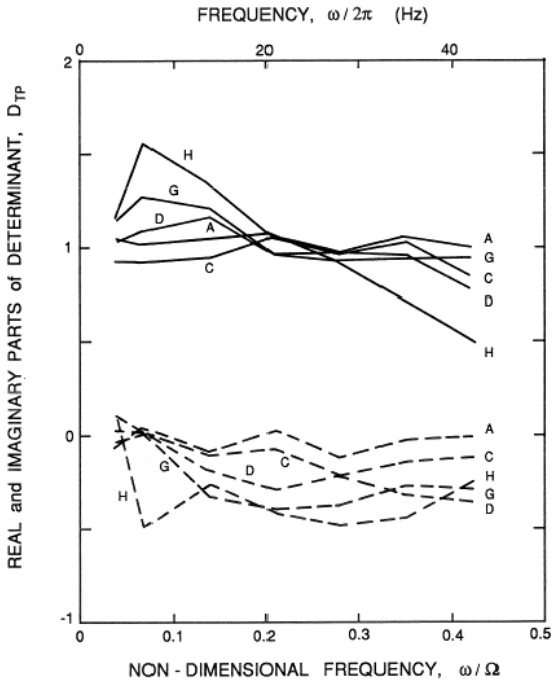

Figure 2: Determinant, D_{TP}, of the experimental transfer functions of figure 1. The real and imaginary parts are shown by the solid and dashed lines respectively and, as in figure 1, the letter code A→H refers to steady state operating points with increasing cavitation (adapted from Brennen *et al.* 1982).

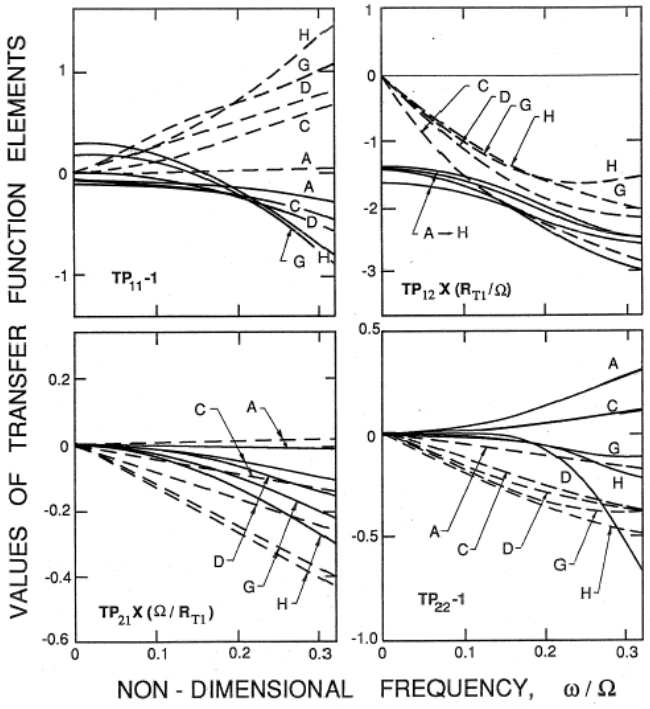

Figure 3: Polynomial curves fitted to the experimental data of figure 1 (adapted from Brennen *et al.* 1982).

described a flow which is nominally steady. We must now consider perturbing both the pressure and the flow rate at inlet, since the relation between these perturbations, and those at discharge, determine the transfer function. Pressure perturbations at inlet will cause pressure waves to travel through the bubbly

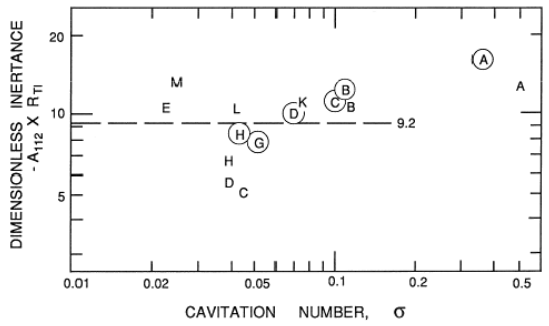

Figure 4: The inertance, $-A_{112}$, non-dimensionalized as $-A_{112}R_{T1}$, as a function of cavitation number for two axial inducer pumps (Impellers IV and VI) with the same geometry but different diameters. Data for the 10.2 *cm* diameter Impeller VI is circled and was obtained from the data of figure 1. The uncircled points are for the 7.58 *cm* diameter Impeller IV. Adapted from Brennen *et al.* (1982).

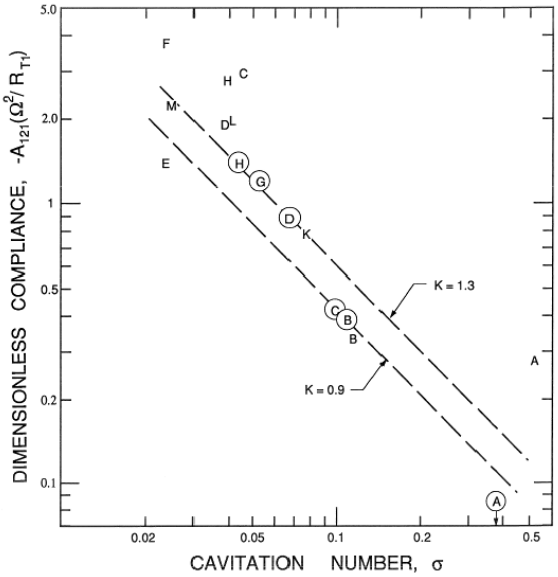

Figure 5: The compliance, $-A_{121}$, nondimensionalized as $-A_{121}\Omega^2/R_{T1}$ for the same circumstances as described in figure 4.

mixture and this part of the process is modeled using a mixture compressibility parameter, K, to determine that wave speed. On the other hand, fluctuations in the inlet flow rate produce fluctuations in the angle of incidence which cause fluctuations in the rate of production of cavitation at inlet. These disturbances would then propagate down the blade passage as kinematic or concentration waves which travel at the mean mixture velocity. This process is modeled by a factor of proportionality, M, which relates the fluctuation in the angle of incidence to the fluctuations in the void fraction. Neither of the parameters, K or M, can be readily estimated analytically; they are, however, the two key features in the bubbly flow model. Moreover they respectively determine the cavitation compliance and the mass flow gain factor, two of the most important factors in the transfer function insofar as the prediction of instability is concerned.

The theory yields the following expressions for A_{111}, A_{112}, A_{121} and A_{122} at small dimensionless frequencies (Brennen 1978, 1982):

$$A_{111}\Omega \simeq \frac{K\zeta\epsilon}{4}\left\{\cot\beta_{b1} + \phi_1/\sin^2\beta_{b1}\right\}$$

$$A_{112}R_{T1} \simeq -\zeta/4\pi\sin^2\beta_{b1}$$

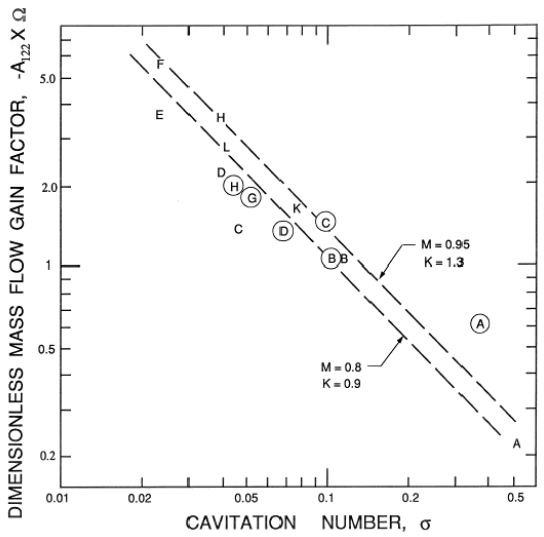

Figure 6: The mass flow gain factor, $-A_{122}$, nondimensionalized as $-A_{122}\Omega$ for the same circumstances as described in figure 4.

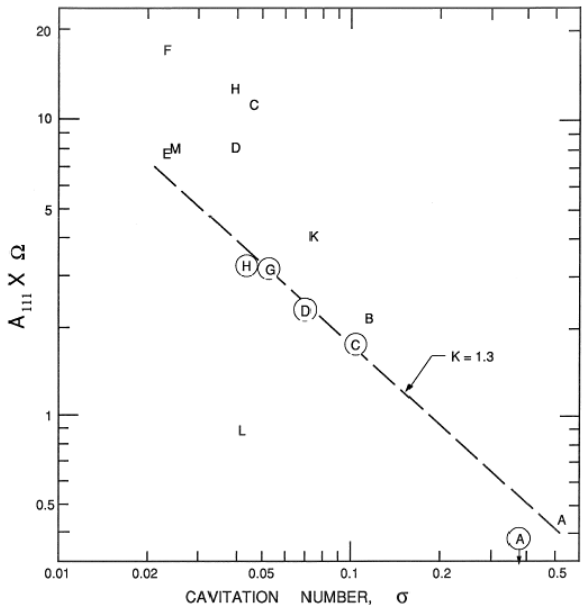

Figure 7: The characteristic, A_{111}, nondimensionalized as $A_{111}\Omega$ for the same circumstances as described in figure 4.

$$A_{121}\Omega^2/R_{T1} \simeq -\pi K\zeta\epsilon/4$$

$$A_{122}\Omega \simeq -\frac{\zeta\epsilon}{4}\left\{M/\phi_1 - K\phi_1/\sin^2\beta_{b1}\right\} \qquad \text{(Bngj3)}$$

where $\zeta = \ell Z_R/R_{T1}$ where ℓ is the axial length of the inducer, and Z_R is the number of blades. Evaluation of the transfer function elements can be effected by noting that the experimental observations suggest $\epsilon \approx 0.02/\sigma$. Consequently, the A_{nij} characteristics from equations (Bngj3) can be plotted against cavitation number. Typical results are shown in figures 4 to 7 for various choices of the two undetermined parameters K and M. The inertance, A_{112}, which is shown in figure 4, is independent of K and M. The calculated value of the inertance for these impellers is about 9.2; the actual value may be somewhat larger because of three-dimensional geometric effects that were not included in the calculation (Brennen *et al.* 1982). The parameter M only occurs in A_{122}, and it appears from figure 6 as though values of this parameter in the

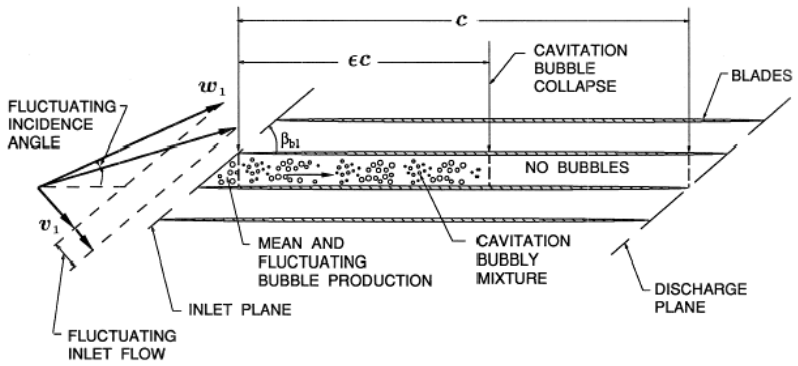

Figure 8: Schematic of the bubbly flow model for the dynamics of cavitating pumps (adapted from Brennen 1978).

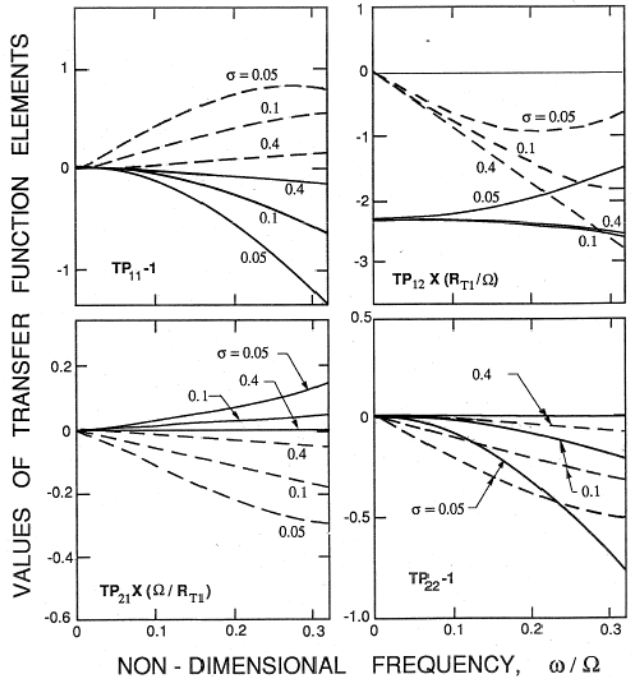

Figure 9: Transfer functions for Impellers VI and IV at $\phi_1 = 0.07$ calculated from the bubbly flow model using $K = 1.3$ and $M = 0.8$ (adapted from Brennen *et al.* 1982).

range $0.8 \rightarrow 0.95$ provide the best agreement with the data. Also, a value of $K \approx 1.3$ seems to generate a good match with the data of figures 5, 6 and 7.

Finally, since $K = 1.3$ and $M = 0.8$ seem appropriate values for these impellers, we reproduce in figure 9 the complete theoretical transfer functions for various cavitation numbers. These should be directly compared with the transfer functions of figure 3. Note that the general features of the transfer functions, and their variation with cavitation number, are reproduced by the model. The most notable discrepancy is in the real part of TP_{21}; this parameter is, however, usually rather unimportant in determining the stability of a hydraulic system. Most important from the point of view of stability predictions, the cavitation compliance and mass flow gain factor components of the transfer function are satisfactorily modeled.